

Resurrect Mask AutoRegressive Modeling for Efficient and Scalable Image Generation

Yi Xin^{1,2,5}, Le Zhuo^{2,3}, Qi Qin², Siqi Luo^{2,4}, Yüewen Cao², Bin Fu², Yangfan He⁶, Hongsheng Li³, Guangtao Zhai⁴, Xiaohong Liu^{4,†} and Peng Gao^{2,†}

¹Nanjing University, ²Shanghai AI Laboratory, ³The Chinese University of Hong Kong, ⁴Shanghai Jiao Tong University,

⁵Shanghai Innovation Institute, ⁶University of Minnesota Twin Cities

AutoRegressive (AR) models have made notable progress in image generation, with Masked AutoRegressive (MAR) models gaining attention for their efficient parallel decoding. However, MAR models have traditionally underperformed when compared to standard AR models. This study refines the MAR architecture to improve image generation quality. We begin by evaluating various image tokenizers to identify the most effective one. Subsequently, we introduce an improved Bidirectional LLaMA architecture by replacing causal attention with bidirectional attention and incorporating 2D RoPE, which together form our advanced model, MaskGIL. Scaled from 111M to 1.4B parameters, MaskGIL achieves a FID score of 3.71, matching state-of-the-art AR models in the ImageNet 256x256 benchmark, while requiring only 8 inference steps compared to the 256 steps of AR models. Furthermore, we develop a text-driven MaskGIL model with 775M parameters for generating images from text at various resolutions. Beyond image generation, MaskGIL extends to accelerate AR-based generation and enable real-time speech-to-image conversion. Our codes and models are available at <https://github.com/synbol/MaskGIL>.

1. Introduction

AutoRegressive (AR) generative models have garnered increasing attention in image generation (Razavi et al., 2019; Esser et al., 2021; Ramesh et al., 2021b; Lee et al., 2022; Yu et al., 2022; Sun et al., 2024; Liu et al., 2024a,b; Bao et al., 2025; Team, 2025), inspired by the success of Transformer (Vaswani, 2017) and GPT (Brown, 2020; OpenAI, 2022; Achiam et al., 2023) in NLP. This paradigm typically unfolds in two stages: the first stage is to quantize an image to a sequence of discrete tokens. In the second stage, an AR model is trained to predict the next token sequentially, based on the previously generated tokens. While AR models exhibit strong generative capabilities, their efficiency is hindered by the extensive number of inference steps, as the AR model *generates one token at a time*.

To overcome this limitation, Mask AutoRegressive (MAR) generative models (Chang et al., 2022; Lezama et al., 2022; Li et al., 2023; Qian et al., 2023; Chang et al., 2023) have been developed, aiming to deliver high-quality image generation with fewer inference steps. Unlike traditional AR models that predict the next token, MAR models *predict a subset of tokens*, offering a potential speed advantage. However, due to the inherent difficulties in training and prediction, the generative capabilities of existing MAR models remain less robust compared to AR models.

In this work, we aim to resurrect Mask Autoregressive (MAR) models for efficient image generation by systematically exploring their capability limits. We begin with an in-depth study to determine the optimal MAR architecture, considering both the choice of image tokenizer and the bidirectional model architecture. Among four prevalent tokenizers, including MaskGIT-VQ (Chang et al., 2022), Chameleon-VQ (Team, 2024), LlamaGen-VQ (Sun et al., 2024), and Open-MAGVIT2-VQ (Luo et al.,

[†] Corresponding author.

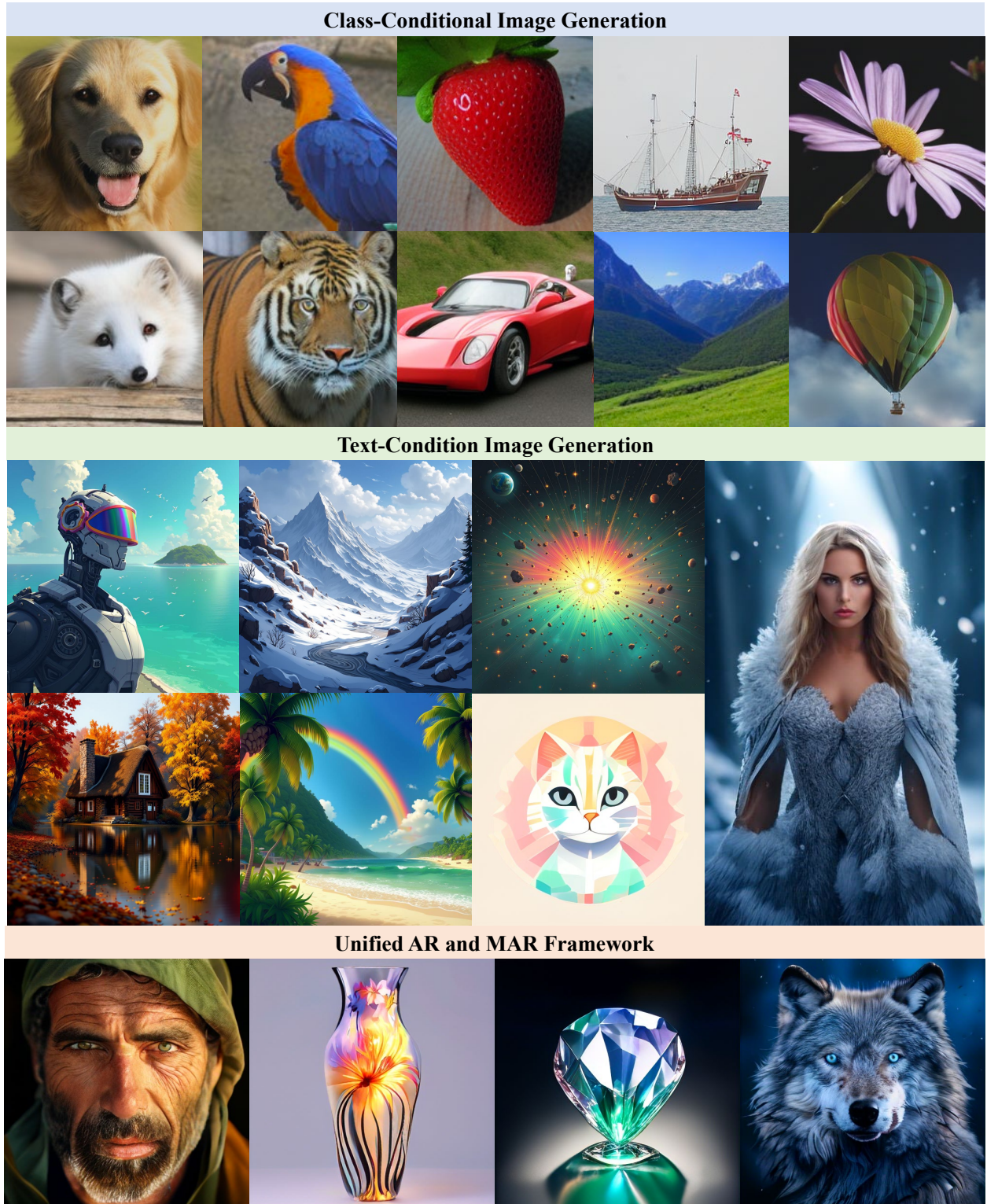


Figure 1: Image Generation with our MaskGIL Model and Unified Inference Framework. We show samples from our class-driven generation (top) and text-driven generation (middle) in various resolutions. At the bottom, we show the generation results of MaskGIL fused with Lumina-mGPT.

2024), we find that LlamaGen-VQ with a codebook size of 16,384 achieves the best performance in

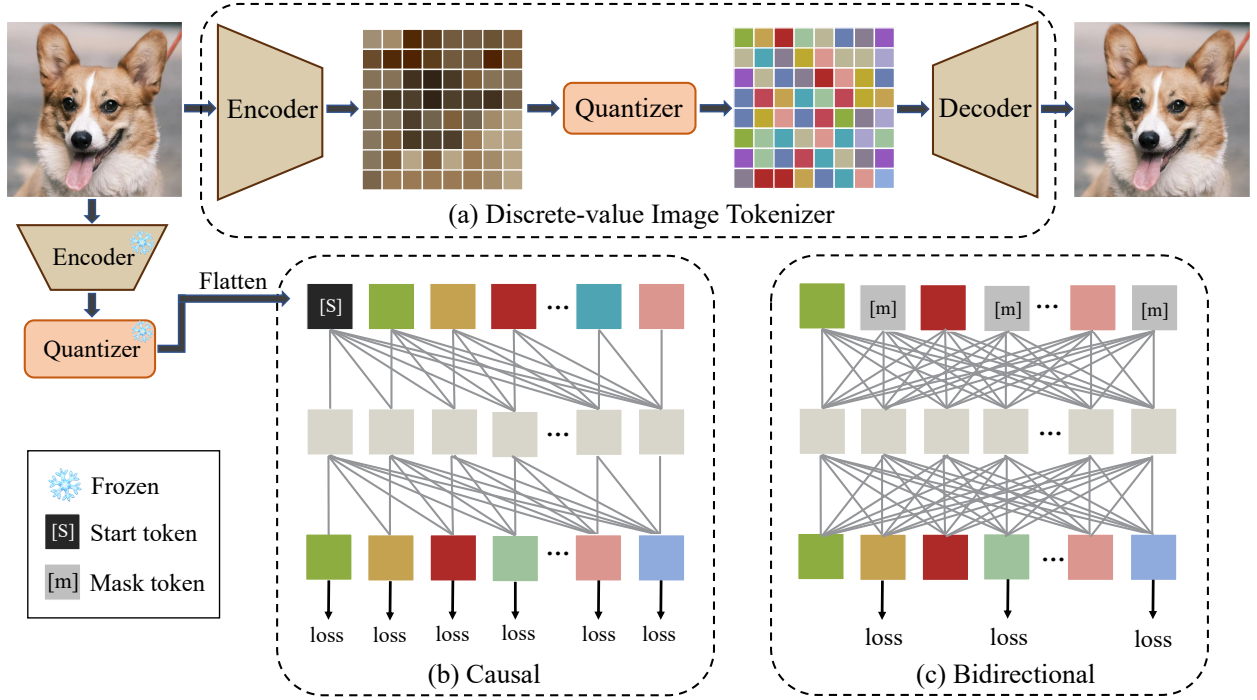


Figure 2: Illustration of (a) discrete-value image tokenizer (encoder and quantizer) and decoder via image reconstruction, (b) training the AR model through causal attention modeling and (c) training the MAR model through bidirectional attention modeling.

MAR-based image generation. Regarding model architecture, inspired by the success of LLaMA (Touvron et al., 2023) in AR generation, we introduce an enhanced Bidirectional LLaMA architecture for MAR, named **Masked Generative Image LLaMA (MaskGIL)**. This enhancement involves modifying causal attention with bidirectional attention and integrating 2D RoPE into every layer of the LLaMA architecture. Through comparative analysis, we find that MaskGIL demonstrates superior image generation capabilities.

Building upon this architecture, we present a series of class-driven image generation models to explore the upper limits of model scaling, ranging from 111M to 1.4B parameters. However, we find that scaling models beyond 1.4B parameters presents significant challenges in maintaining stable training. To address this issue, we incorporate query-key normalization (QK-Norm) and Post-Norm, which effectively stabilize training at larger scales. Furthermore, we introduce a text-driven image generation model with 775M parameters, capable of flexibly generating images at various resolutions while maintaining high quality.

In addition to focusing on the fundamental image generation capabilities of MaskGIL, we have also expanded MaskGIL to broader applications, including: (1) **Accelerating AR Generation:** We propose a hybrid framework that leverages an AR model to generate a portion of the tokens, which then serve as prompts for MaskGIL to complete the remaining tokens. This hybrid approach significantly reduces the number of AR sampling steps while maintaining high visual fidelity. (2) **Real-Time Speech-To-Image Generation System:** The fast sampling strategy of MaskGIL makes it more suitable for interactive generation with users compared to pure AR generation. Therefore, we develop a real-time speech-to-image generation system based on our MaskGIL model. In summary, our contributions include:

- **Exploring the Optimal Design of Mask AutoRegressive Model.** We conduct a comprehensive

study to evaluate the impact of different image tokenizers on image generation, aiming to identify the most effective tokenizer. Furthermore, we introduce an improved Bidirectional LLaMA model, which ultimately defines the optimal MAR architecture.

- **Scaling Mask AutoRegressive Model.** Building upon the optimal MAR generative architecture, we introduce a series of class-driven image generation models with parameter sizes ranging from 111M to 1.4B. Our largest model attains an FID score of 3.71 on the ImageNet 256×256 benchmark with merely 8 inference steps. Furthermore, we develop a text-to-image model with 775M parameters, enabling the efficient synthesis of high-fidelity photorealistic images at arbitrary resolutions.
- **Extending MAR to Accelerate AR Generation.** To achieve both high efficiency and superior image quality, we introduce a fusion framework that integrates the AR and MAR paradigms during inference. By leveraging partially generated tokens from AR as initialization for MAR, our approach facilitates a seamless transition between these two paradigms, offering a flexible trade-off between computational efficiency and generation fidelity. Notably, our framework reduces generation time by over 70+% while delivering results comparable to state-of-the-art AR models.
- **Real-Time Speech-To-Image Generation System.** We develop a real-time speech-to-image generation system, wherein speech inputs are first translated into English text using Whisper, a multilingual speech recognition model supporting over 90 languages. The translated text then serves as a prompt to guide the MAR model in generating corresponding images, which are subsequently returned to the user.

2. Preliminaries

2.1. Discrete-Value Image Tokenizer

To begin with, we revisit the discrete-value image tokenizer, which plays a crucial role in both AR and MAR image generation. The most commonly used tokenizer is the VQ-VAE (Van Den Oord et al., 2017), an encoder-quantizer-decoder architecture, as shown in Figure 2(a). This architecture employs a ConvNet for both the encoder and decoder, featuring a downsampling ratio p . The encoder projects the image pixels $x \in \mathbb{R}^{H \times W \times 3}$ to a feature map $f \in \mathbb{R}^{h \times w \times C}$, where $h = H/p$ and $w = W/p$. The core of this process lies in the quantizer, which includes a codebook $Z \in \mathbb{R}^{K \times C}$ with K learnable vectors. Each vector $f^{(i,j)}$ in the feature map is mapped during quantization to the code index $q^{(i,j)}$ of its nearest vector z^k in the codebook. Consequently, the image pixels $x \in \mathbb{R}^{H \times W \times 3}$ are quantized into $q \in \mathbb{Q}^{h \times w}$. During the decoding phase, the code index $q^{(i,j)}$ is remapped to the feature vector and the decoder converts these feature vectors back to the image pixels \hat{x} . There are various works (Razavi et al., 2019; Esser et al., 2021; Yu et al., 2023) that continue to explore the design of VQ-VAE for improving reconstruction quality.

2.2. AutoRegressive Generative Models

AutoRegressive models revolutionize the fields of language modeling (Brown et al., 2020; Achiam et al., 2023; Team et al., 2023; Touvron et al., 2023; Meta, 2024) and multimodal understanding (Liu et al., 2023; Lin et al., 2023; Team, 2024) using the unified *next-token prediction paradigm for all modalities with a casual transoformer*, as illustrated in Figure 2(b).

This paradigm has been extended to the visual generation domain by early works such as DALL-E (Ramesh et al., 2021a), Cogview (Ding et al., 2021), and Parti (Yu et al., 2022). These works leverage a two-stage approach where the image tokenizer first encodes continuous images into discrete tokens then the transformer decoder models the flattened one-dimensional sequences. During

Table 1: Reconstruction performance and codebook usage of different discrete-value image tokenizers. All tokenizers employ a downsampling ratio of 16 and are trained on the ImageNet training set at a training resolution of 256×256 .

Method	Year	Ratio	Train Resolution	Codebook Size	rFID↓	Codebook Usage↑
MaskGIT-VQ (Besnier and Chen, 2023)	2023	16×16	256×256	1024	10.79	44.3%
Chameleon-VQ (Team, 2024)	2024	16×16	256×256	8192	8.34	38.3%
LlamaGen-VQ (Sun et al., 2024)	2024	16×16	256×256	16384	4.54	100%
Open-MAGVIT2-VQ (Luo et al., 2024)	2024	16×16	256×256	262144	4.03	100%

training, the casual transformer is trained to predict the categorical distribution $p_{\theta}(x_i \mid x_{<i}; c)$ at each position conditioned on the additional information c , e.g., text prompts or class labels. During inference, image token sequences can be sampled in the same way as language generation and further decoded back to pixels. Despite this simple and unified paradigm for image synthesis, AR-based visual generative models have long been overlooked for a while, particularly after the exploding of diffusion models. One potential reason is their inferior generation quality restricted by the image tokenizer. Recently, LlamaGen (Sun et al., 2024) improves the design of image tokenizer and leverages the Llama architecture for scaling, which enhance the performance of autoregressive models.

2.3. Mask AutoRegressive Generative Models

Different from the next token prediction paradigm typical of autoregressive generation, mask autoregressive models (Chang et al., 2022; Li et al., 2023; Chang et al., 2023) leverage a *bidirectional transformer to simultaneously generate all visual tokens through a masked-prediction mechanism*, as illustrated in Figure 2(c).

These models are trained using a proxy task similar to the mask prediction task employed in BERT (Kenton and Toutanova, 2019). In this setup, bidirectional attention allows all known tokens to see each other while also permitting all unknown tokens to view all known tokens, enhancing communication across tokens compared to causal attention. In contrast to causal attention, where training loss is computed on sequentially revealed tokens, MAR models compute the loss solely on the unknown tokens. At inference time, these models utilize a novel decoding method that synthesizes an image in a constant number of steps, typically between 8 and 15 (Chang et al., 2022). Specifically, during each iteration, the model predicts all tokens in parallel, retaining only those predicted with high confidence. Less certain tokens are masked and re-predicted in subsequent iterations. This process repeats, progressively reducing the mask ratio until all tokens are accurately generated through several refinement iterations.

3. Exploring the Optimal Design of Mask AutoRegressive Models

3.1. Rethinking Image Tokenizer For High-Quality Generation

For high-quality image generation, the choice of a discrete-value image tokenizer is critical, as it determines the upper limit of the generation quality. Various tokenizers have been developed, and in this study, we evaluate four recent mainstream tokenizers, including MaskGIT-VQ (Besnier and Chen, 2023), Chameleon-VQ (Team, 2024), LlamaGen-VQ (Sun et al., 2024), and Open-MAGVIT2-VQ (Luo et al., 2024), as shown in Table 1. All tokenizers use a downsampling ratio of 16×16 and are trained on the ImageNet (Deng et al., 2009). We conduct detailed experiments using both AR and MAR

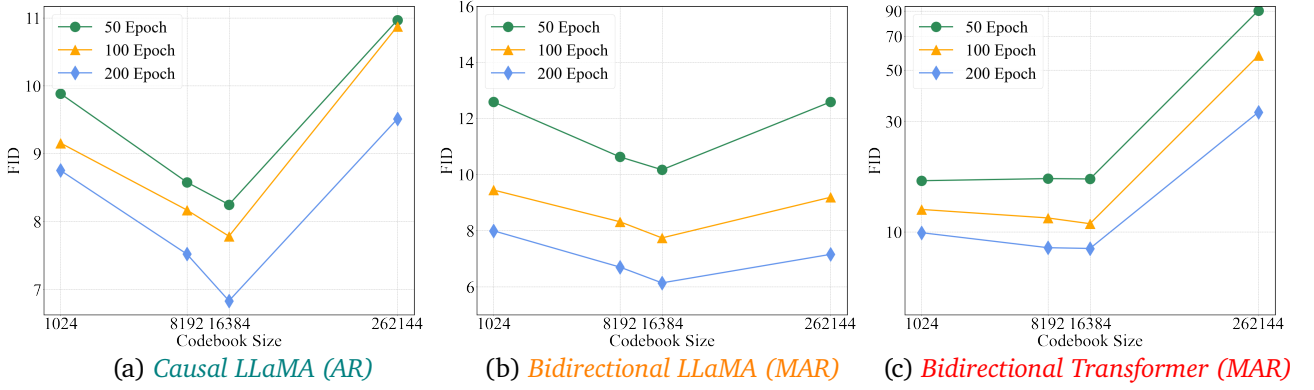


Figure 3: Visual Generation Evaluation. We show FID of class-driven ImageNet 256×256 benchmark over training epochs.

frameworks to provide comprehensive insights into image tokenizers.

3.1.1. Visual Reconstruction Evaluation

Before assessing the impact of the image tokenizer on generation quality, we initially focus on evaluating the performance of each tokenizer itself. We analyze the reconstruction quality and codebook utilization using the ImageNet validation set, with results detailed in Table 1. From the results, we can find that as the codebook size increases, the relative rFID¹ value decreases, indicating that the reconstruction image quality is gradually improving. However, when the codebook size reaches a certain level, the improvement in the reconstructed image quality is limited. For instance, despite Open-MAGVIT2-VQ expanding its codebook size $16\times$ compared to LlamaGen-VQ, the rFID reduction is a mere 0.51, indicating that blindly increasing the codebook size for the sole purpose of improvement is not a wise choice in the design of a discrete-value image tokenizer. In terms of codebook utilization, LlamaGen-VQ and Open-MAGVIT2-VQ achieve 100%, which is due to replacing traditional code assignment (*i.e.*, pair-wise distance) with lookup-free quantization (Luo et al., 2024).

3.1.2. Visual Generation Evaluation

Evaluation Setting. To explore the impact of image tokenizers on image generation, we conduct detailed experiments using four tokenizers across two paradigms: AutoRegressive (AR) and Mask AutoRegressive (MAR) generation. For AR generation, we utilize the advanced LLaMA as the foundational architecture, consistent with LlamaGen (Sun et al., 2024). For MAR generation, following MaskGIT (Chang et al., 2022), we employ the Bidirectional Transformer model as the foundational architecture and also modify LLaMA to a bidirectional variant. To facilitate a fair comparison between these foundational models, both the Transformer and LLaMA architectures are configured under identical conditions ($\sim 100M$ parameters): 12 layers, 12 heads, and 768 dimensions. All experiments are conducted on the class-driven image generation ImageNet benchmark with 256×256 resolution and trained for 200 epochs. During the evaluation, we generate 50,000 images across 1,000 classes, with 50 images per class. We employ FID and Inception Score (IS) as evaluation metrics, consistent with previous studies (Li et al., 2024b).

Evaluation Results. The evaluation results are shown in Figure 3, and the detailed results are shown

¹The reconstruction Fréchet inception distance, denoted as rFID (Heusel et al., 2017), is usually adopted to measure the quality of reconstructed images.

Table 2: Model sizes and architecture configurations of MaskGIL models. The configurations are following previous works (Sun et al., 2024; Touvron et al., 2023; OpenLM-Research, 2023). We replace causal attention to bidirectional attention for MAR modeling. We add QK-Norm and Post-Norm for stable training.

Model	Parameters	Layers	Hidden Size	Heads	QK-Norm	Post-Norm
MaskGIL-B	111M	12	768	12	✗	✗
MaskGIL-L	343M	24	1024	16	✗	✗
MaskGIL-XL	775M	36	1280	20	✗	✗
MaskGIL-XXL	1.4B	48	1536	24	✓	✓

in Appendix A. Based on the results, LlamaGen-VQ emerges as the superior choice, delivering the best performance in both AR and MAR image generation tasks. Open-MAGVIT2-VQ, which performs best in the reconstruction evaluation, delivers unsatisfactory results in image generation quality, especially on the Transformer architecture of the MAR generation task, where it performs very poorly. As for Chameleon-VQ, although it is widely adopted in many previous image generation works (Team, 2024; Liu et al., 2024a), its performance does not match that of LlamaGen-VQ. Therefore, our exploration provides guidance for the selection of image tokenizers, suggesting that LlamaGen-VQ may be a better choice.

Discussion. Our evaluation focuses on generative models with $\sim 100\text{M}$ parameters, providing a valuable benchmark. While we acknowledge the possibility that scaling model parameters, Open-MAGVIT2-VQ, with its 262,144 codebook size, could potentially yield better performance. However, its high training complexity, large parameters for the classification head, and significant GPU resource demands make it impractical for many real-world applications. Furthermore, all evaluations are only conducted on class-driven generation tasks, which may introduce a slight bias to our experimental results, but this limitation has minimal impact on the overall conclusions.

3.2. Optimized Mask Autoregressive Model Architecture

In Section 3.1, we investigate the influence of image tokenizers on generation quality and identify LlamaGen-VQ as the most effective tokenizer. To further optimize the MAR architecture, we introduce a Bidirectional LLaMA architecture, inspired by the state-of-the-art AR-based model (Sun et al., 2024), referred to as **Masked Generative Image LLaMA (MaskGIL)**. Specifically, we modify causal attention with bidirectional attention and integrate 2D RoPE into every layer of the LLaMA architecture. Moreover, we omit the use of the AdaLN technique (Peebles and Xie, 2023) to preserve alignment with the standard LLM architecture. A comparison between our *Bidirectional LLaMA* and the *Bidirectional Transformer* used in the previous MAR generation, as depicted in Figure 3, demonstrates that the Bidirectional LLaMA consistently achieves superior generation quality.

4. Resurrect Mask AutoRegressive Model

Numerous studies have extensively explored AR generation, with prominent works such as LlamaGen (Sun et al., 2024), which successfully scaled AR models to 3B parameters. In contrast, the scaling of MAR models remains relatively underexplored, primarily due to their performance gap compared to AR models. However, our optimized MaskGIL architecture effectively bridges this gap, resurrecting the MAR generation paradigm and unlocking its potential for broader applications.

4.1. Model Scaling

Scaling Mask AutoRegressive Model. Previous research on MAR image generation (Chang et al., 2022; Li et al., 2023) has primarily focused on models with parameter sizes ranging between 200M and 300M, with limited exploration into scaling to larger model sizes. In this study, we examine the relationship between the generation performance of MAR models and model scaling by increasing the parameter size of our MaskGIL from 111M to 1.4B on the class-driven ImageNet generation benchmark. The detailed configurations of our MaskGIL models, with varying parameter sizes, are provided in Table 2. Additionally, we develop text-driven MaskGIL models with 775M parameters, capable of generating images at any resolution according to the text descriptions.

Training Stability. Scaling MaskGIL models beyond 1.4B parameters presents significant challenges in maintaining stable training, as instabilities often arise during the late stages of training. This observation is consistent with findings from several prior studies (Dehghani et al., 2023; Team, 2024; Gao et al., 2025; Zhuo et al., 2024). The fundamental reason stems from the standard LLaMA architecture for visual modeling, which exhibits complex divergences due to slow norm growth during the mid-to-late stages of training. To address this problem, we adopt query-key normalization (QK-Norm) (Team, 2024; Dehghani et al., 2023) and Post-Norm (Zhuo et al., 2024). QK-Norm involves applying layer normalization to the query and key vectors within the attention mechanism, while Post-Norm applies layer normalization to the outputs of both the attention and MLP layers. Together, these techniques effectively mitigate uncontrollable norm growth caused by unnormalized pathways, thereby stabilizing the training process and enabling the successful scaling of MaskGIL models.

4.2. Robust and Efficient Inference Strategy

Classifier-Free Guidance. Classifier-Free Guidance (CFG) (Ho and Salimans, 2021; Sanchez et al., 2023) was initially introduced to enhance the quality and text alignment of generated samples in text-to-image diffusion models. We incorporate this technique into our MaskGIL models. During training, the conditional input is randomly dropped and replaced with a null unconditional embedding (Liu et al., 2024a; Zhuo et al., 2024; Yi et al., 2024; Zhuo et al., 2025; Qin et al., 2025). During inference, for each image token, CFG modifies the logits ℓ_{cfg} , which are defined as $\ell_{cfg} = \ell_u + s(\ell_c - \ell_u)$. Here, ℓ_c represents the conditional logits, ℓ_u denotes the unconditional logits, and s is the scale factor for the classifier-free guidance. As illustrated in Figure 4(b), CFG substantially influences the performance of MaskGIL models.

Iterative Decoding. Despite the bidirectional architecture of MaskGIL enabling one-step image generation, the generated images might lack sufficient quality. To address this, we adopt the iterative decoding strategy proposed in (Chang et al., 2022), which facilitates image generation over T steps, typically ranging from 8 to 16. **At each iteration, the model predicts all tokens simultaneously but retains only the most confident predictions.** Tokens with lower confidence are masked and re-predicted in subsequent iterations, with the mask ratio progressively decreasing until all tokens are generated within the designated T iterations.

To generate an image, we begin with a blank canvas where all tokens are initially masked, denoted as $Y_M^{(0)}$. At iteration t , the iterative decoding algorithm proceeds as follows:

- **Step 1: Predict.** Given the masked tokens $Y_M^{(t)}$ at the current iteration, the model predicts the probabilities, denoted as $p^{(t)} \in \mathbb{R}^{N \times K}$, for all masked locations in parallel.
- **Step 2: Sample.** For each masked location i , a token $y_i^{(t)}$ is sampled based on its prediction probabilities $p_i^{(t)} \in \mathbb{R}^K$ over all possible tokens in the codebook. The corresponding predic-

Table 3: Model comparisons on class-conditional ImageNet 256×256 benchmark. “Step” indicates the number of inference steps. Metrics include FID, IS, Precision and Recall. “↓” or “↑” indicate lower or higher values are better. † indicates that the result comes from the original paper.

Type	Model	#Param.	Steps↓	FID↓	IS↑	Precision↑	Recall↑
AR	RQTransformer† (Lee et al., 2022)	3.8B	256	7.55	134.00	—	—
	LlamaGen-B† (Sun et al., 2024)	111M	256	5.46	193.61	0.83	0.45
	LlamaGen-L† (Sun et al., 2024)	343M	256	3.07	256.06	0.83	0.52
	LlamaGen-XL† (Sun et al., 2024)	775M	256	2.62	244.08	0.80	0.57
	LlamaGen-XXL† (Sun et al., 2024)	1.4B	256	2.34	253.90	0.80	0.59
MAR	MaskGIT† (Chang et al., 2022)	227M	8	6.18	182.1	0.80	0.51
	MAGE† (Li et al., 2023)	230M	20	6.93	195.8	—	—
MAR	MaskGIL-B (CFG=2.0)	111M	8	5.64	229.96	0.83	0.48
	MaskGIL-L (CFG=2.0)	343M	8	4.01	281.11	0.84	0.51
	MaskGIL-XL (CFG=2.5)	775M	8	3.90	296.25	0.87	0.49
	MaskGIL-XXL (CFG=2.5)	1.4B	8	3.71	303.47	0.88	0.52

tion score is used as a confidence score, representing the model’s certainty in the prediction. Confidence scores for unmasked positions in $Y_M^{(t)}$ are set to 1.0.

- **Step 3: Mask Schedule.** The number of tokens to be masked is determined by the mask scheduling function γ , computed as $n = \lceil \gamma(\frac{t}{T})N \rceil$, where N is the input length and T is the total number of iterations. In this work, we design five types of mask schedules: Root Schedule, Linear Schedule, Cosine Schedule, Square Schedule, and Arccos Schedule. For detailed descriptions of these schedules, please refer to Appendix B.
- **Step 4: Mask.** The updated masked tokens $Y_M^{(t+1)}$ are obtained by masking n tokens in $Y_M^{(t)}$. The mask $M^{(t+1)}$ for iteration $t + 1$ is calculated as:

$$m_i^{(t+1)} = \begin{cases} 1, & \text{if } c_i < \text{sorted}_j(c_j)[n], \\ 0, & \text{otherwise.} \end{cases},$$

where c_i is the confidence score for the i -th token.

4.3. Class-Driven Image Generation

Training and Evaluation Setup. The class embedding is derived from a set of learnable embeddings (Li et al., 2024a; Esser et al., 2021) and serves as the prefilling token embedding. From this initial token embedding, the model generates all image tokens. We conduct class-driven generation experiments on the ImageNet dataset. All models are trained for token unmasking using cross-entropy loss with a label smoothing factor of 0.1. The optimizer used is AdamW with a learning rate of $1e^{-4}$, betas=(0.9, 0.96), and a weight decay of $1e^{-5}$. For classifier-free guidance, the dropout rate for the class condition embedding is set to 0.1. All models are trained with a batch size of 256. In addition to evaluating performance with the FID and IS metrics, we also report Precision and Recall (Kynkäänniemi et al., 2019) to provide a more comprehensive evaluation.

Comparisons with Other Class-Driven Generation Models. In Table 3, we compare our model against popular AR and MAR image generation models, including RQTransformer (Lee et al., 2022), LlamaGen (Sun et al., 2024), MaskGIT (Chang et al., 2022), and MAGE (Li et al., 2023). Our

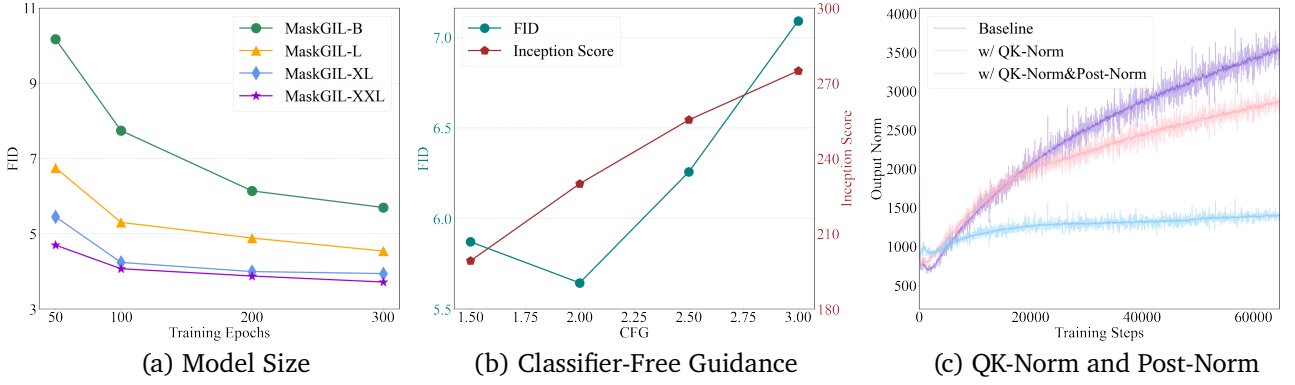


Figure 4: The Effect of Model Size, CFG, QK-Norm, and Post-Norm. We show the FID scores on the ImageNet benchmark across different model sizes and CFG configurations. Scaling the model size consistently improves FID scores throughout the training process. The impact of CFG is also notable. To monitor training stability, we plot the model’s output norm.

MaskGIL models achieve competitive performance across all metrics, including FID, IS, Precision, and Recall. **Importantly, MaskGIL requires only 8 inference steps, underscoring its efficiency in image generation.** Further details on inference steps are provided in Appendix C. While the FID and Recall scores of MaskGIL are slightly lower than those of LlamaGen, it achieves higher IS and Precision scores. This result indicates a trade-off between diversity and visual quality in the generated images, which could potentially be mitigated by exploring more advanced sampling strategies.

Effective of Model Size. We train our MaskGIL models across four model sizes (B-111M, L-343M, XL-775M, XXL-1.4B) and evaluate their performance in Table 3. Figure 4(a) depicts the changes in FID as both model size and training epochs increase. Significant improvements in FID are observed when scaling the model from MaskGIL-B to MaskGIL-XL. However, further scaling to 1.4B results in only marginal gains. A plausible explanation for this phenomenon is that the ImageNet dataset size may constrain the performance improvements achievable through model scaling (Sun et al., 2024).

Effective of Classifier-Free Guidance. Figure 4(b) presents the FID and IS scores of MaskGIL-L under various classifier-free guidance (CFG) settings. MaskGIL-L achieves its best FID at CFG = 2.0, and increasing CFG beyond this point results in a deterioration in FID, which aligns with previous findings (Dhariwal and Nichol, 2021; Sun et al., 2024). This demonstrates that CFG plays a crucial role in influencing the generation performance of our MaskGIL models. For further results on different model sizes, please refer to Appendix D.

Effective of QK-Norm and Post-Norm. In Figure 4(c), we show the output norm of the MaskGIL-XXL (1.4B) with and without QK-Norm/Post-Norm. Without QK-Norm and Post-Norm, the output norm grows uncontrollably, leading to non-convergence and the occurrence of “nan” loss values during the training. Normalizing the query and key embeddings before computing the attention matrix helps to avoid attention collapse but merely mitigates this norm growth. Ultimately, the inclusion of both QK-Norm and Post-Norm ensures the output remains stable, preventing dramatic increases and resulting in more stable training for scaling.

Ablation Study on Different Iterative Decoding Schedules. We evaluate five mask schedulers: Root, Linear, Square, Cosine, and Arccos (details in Appendix B). We conduct a comparative analysis of these schedulers on the ImageNet benchmark, as presented in Figure 5(f). The results indicate that among all schedulers, the arccos scheduler achieves the best FID, while the root scheduler attains the best IS. Overall, we recommend using the arccos scheduler.

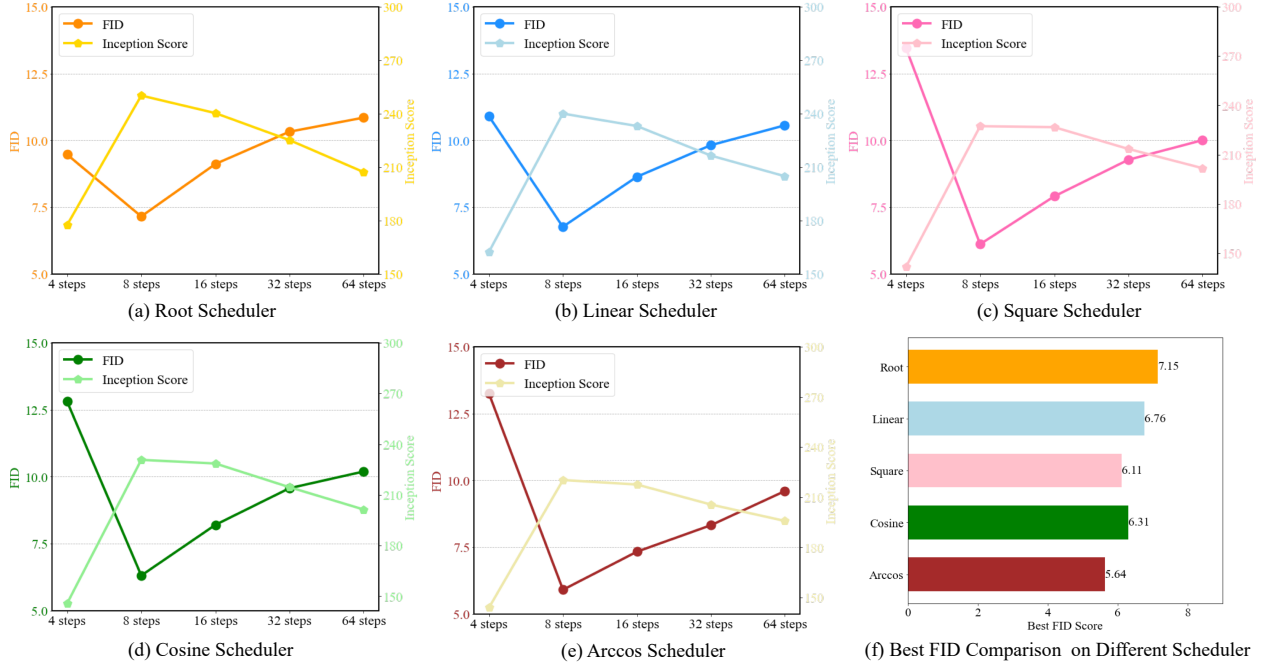


Figure 5: Performance Comparison of Different Decoding Steps and Different Schedulers. This experiment shows the checkpoint results of MaskGIL-B at 400 epochs, with CFG= 2.0.

Table 4: Performance comparison across different T2I models on GenEval benchmark.

Methods	# Params	Single Obj.	Two Obj.	Counting	Colors	Position	Color Attri.	Overall \uparrow
Diffusion Models								
SDv1.5 (Rombach et al., 2022)	0.9B	0.97	0.38	0.35	0.76	0.04	0.06	0.43
SDv2.1 (Rombach et al., 2022)	0.9B	0.98	0.51	0.44	0.85	0.07	0.17	0.50
PixArt- α (Chen et al., 2023)	0.6B	0.98	0.50	0.44	0.80	0.08	0.07	0.48
AutoRegressive Models								
LlamaGen (Sun et al., 2024)	0.8B	0.71	0.34	0.21	0.58	0.07	0.04	0.32
Chameleon (Team, 2024)	7B	-	-	-	-	-	-	0.39
Lumina-mGPT (Liu et al., 2024a)	7B	0.98	0.77	0.27	0.82	0.17	0.32	0.56
MaskGIL (Ours)	0.7B	0.98	0.52	0.24	0.69	0.24	0.29	0.49

Ablation Study on Decoding Steps. In Table 3, all experimental results are based on an 8-step decoding process. To investigate how the number of decoding steps affects generation quality, we conduct an ablation study on the class-driven ImageNet benchmark, with findings illustrated in Figure 5(a)-(e). The results reveal a consistent trend across all mask schedulers: increasing the number of decoding steps does not always lead to improved generation quality. Notably, the 8-step decoding process achieves the best results across all schedulers.

4.4. Text-Driven Image Generation

Image and Text Tokenizer. While we evaluate the effectiveness of the LlamaGen-VQ tokenizer for class-driven generation, its application in text-driven generation remains unexplored due to its high resource consumption. Therefore, for text-driven generation, we adopt the Chameleon-VQ tokenizer, which is consistent with the advanced AR model. This choice also facilitates the exploration of AR

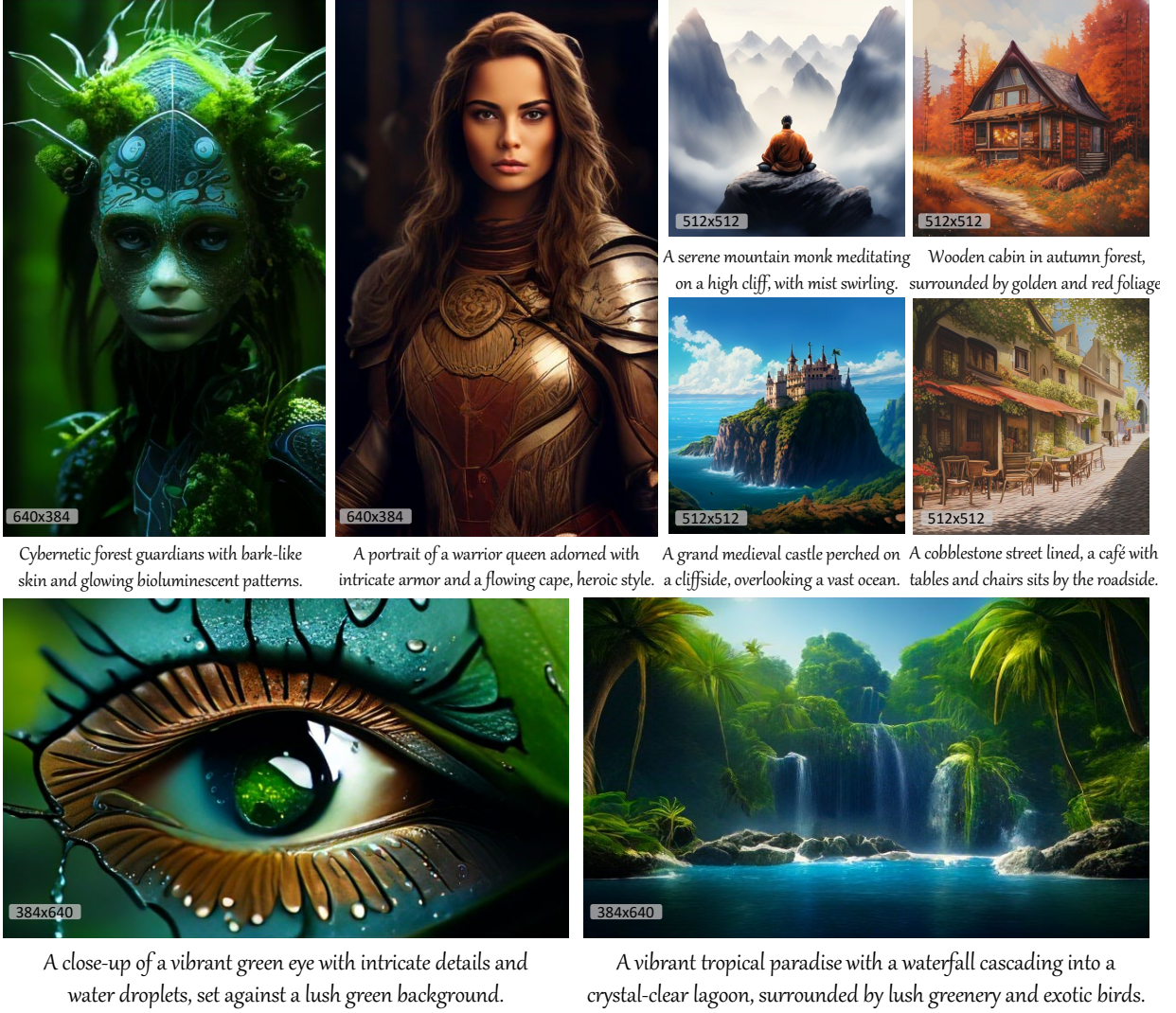


Figure 6: Visualization of text-driven image generation. The prompts are generated by GPT-4. MaskGIL can generate images at any resolution while preserving consistency with the text.

and MAR integration, as discussed in Section 5.1. To incorporate text prompts into our MaskGIL model, we utilize Gemma-2B (Team et al., 2024) as the text encoder. Gemma-2B offers performance comparable to large-scale LLMs while maintaining high efficiency. The extracted text features are subsequently processed through an additional MLP and used as prefilling token embeddings within MaskGIL.

Training and Evaluation Setup. The training dataset consists of 2M high-aesthetic images with prompts generated by a mixture of captioners. We employ a two-stage progressive training pipeline, initially training on 256×256 resolution before transitioning to 512×512 . To enable image generation with arbitrary aspect ratios, we adopt a multi-resolution training strategy by defining a series of size buckets and resizing each image to its nearest bucketed shape. All other training hyperparameters follow the class-driven settings. We employ standard GenEval (Ghosh et al., 2024) benchmark to evaluate MaskGIL. These metrics primarily assess text-image alignment.

Quantitative Performance. As shown in Table 4, MaskGIL achieves competitive performance compared to existing AR and Diffusion models, obtaining an overall score of 0.49 on the GenEval

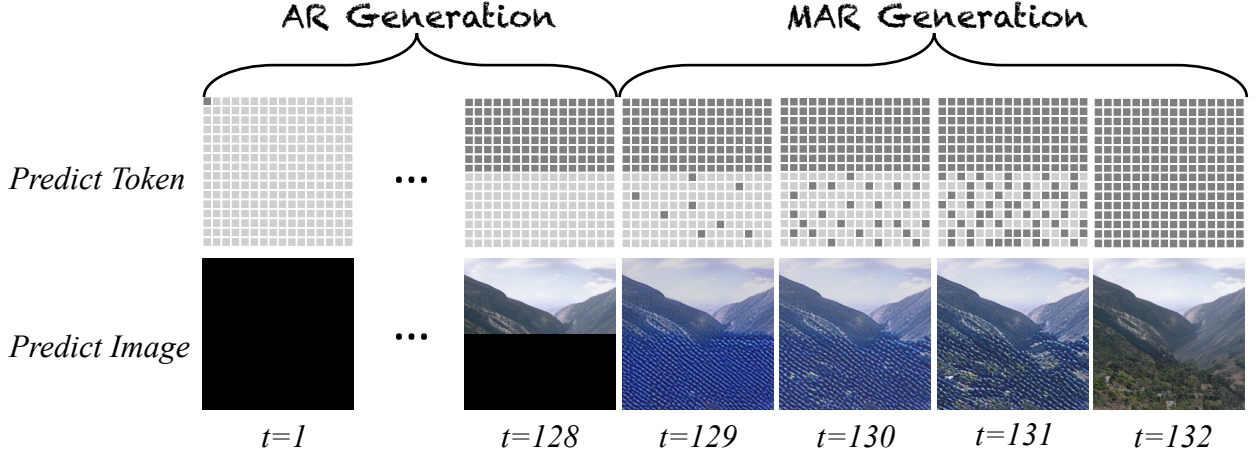


Figure 7: Illustration of our unified framework. This framework initially employs AR to generate a subset of image tokens. Subsequently, MAR is deployed to complete the generation of the remaining tokens. In this example, only 132 inference steps are needed, of which AR takes 128 steps.

benchmark. It surpasses LlamaGen and Chameleon but still lags behind the state-of-the-art model Lumina-mGPT. The primary factors contributing to this gap between MaskGIL and Lumina-mGPT are: 1) **Limited Training Data:** MaskGIL was trained on a significantly smaller dataset. 2) **Model Size:** MaskGIL contains only 0.7B parameters, whereas Lumina-mGPT has 7B parameters. If these two challenges are addressed—by scaling up training data and increasing model size—MaskGIL’s capability in text-driven image generation is expected to improve significantly.

Qualitative Performance. In Figure 6, we use prompts randomly generated by GPT-4o to create images at various resolutions. MaskGIL demonstrates strong text-to-image generation capabilities, producing high-quality images across diverse styles and subjects while maintaining excellent text alignment. In future work, we plan to extend support for higher resolution generation, such as 1024×1024 .

5. Application of MaskGIL

5.1. Extending MaskGIL to Accelerate AR Generation

From the exploration of AR and MAR generation paradigms above, it is evident that AR models excel in producing high-quality images, while MAR models offer the advantage of fast generation speed. To achieve both rapid and high-fidelity image generation, we propose a unified inference framework that integrates AR models with our MaskGIL, as shown in Figure 7. We validate this framework on both class-driven and text-driven image generation tasks.

Unified Inference Framework for Integrating AR and MAR. In this work, we extensively explore and optimize the generative capabilities of MAR models. However, despite these advancements, a performance gap remains when compared to AR models, as demonstrated in Table 3 and Table 4. Drawing inspiration from recent research (Li et al., 2024b), which suggests that AR and MAR paradigms can be unified into a single generative framework, we propose a novel inference strategy that leverages the strengths of both approaches. As illustrated in Figure 7, the proposed framework begins by employing AR models to generate a subset of image tokens, which serve as image/token prompts. These prompts are then used as input by MAR models to complete the generation of the



Figure 8: Generated images and time consumption at different ratios of inference steps of Lumina-mGPT. Our unified framework reduces generation time while ensuring quality.

remaining tokens. This hybrid approach enables efficient image generation while preserving high visual fidelity, effectively bridging the gap between speed and quality.

Evaluation on Class-Driven Image Generation.

We use LlamaGen-L (Sun et al., 2024) (343M parameters) as the base class-driven AR model. To clearly demonstrate the effectiveness of our unified framework, we select a smaller MaskGIL-B model (111M parameters) as the MAR model. For evaluation, we measure the FID score on the ImageNet dataset, with the CFG scale set to 2.0. The experimental results are presented in Table 5. We observe that when integrating MaskGIL-B with LlamaGen-L at different AR generation ratios, the FID score increases from 3.80 (for pure LlamaGen-L) to 5.64 (for pure MaskGIL). This trend indicates that while introducing the MAR model accelerates sampling, it comes at the cost of reduced image quality. These findings highlight the need to maintain a fundamental trade-off between sample efficiency and generation quality.

Table 5: Experimental Results of Sampling Steps and FID on ImageNet. “AR Ratio” refers to the proportion of sampling steps performed by the AR model relative to the initial total of 256 steps.

Method	AR Ratio	Sample Steps	FID↓
LlamaGen-L	100%	256	3.80
+ MaskGIL	75%	200 (+21.9%)	3.96 (-4.21%)
+ MaskGIL	50%	136 (+46.9%)	4.23 (-11.31%)
+ MaskGIL	25%	72 (+71.9%)	4.68 (-23.16%)
+ MaskGIL	0%	8 (+96.9%)	5.64 (-48.42%)



Figure 9: Speech-to-Image Generation System.

Evaluation on Text-Driven Image Generation. We use Lumina-mGPT (Liu et al., 2024a) (7B parameters) as the base text-driven AR model, known for its capability to generate flexible and photorealistic images from text descriptions. For the MAR model, we leverage our MaskGIL with 775M parameters. However, since MaskGIL currently supports generation only at a 512×512 resolution, our experiments are constrained to this resolution. The CFG scale for the experiments is set to 4.0. In Figure 8, we present examples along with inference times for images generated using our unified framework. The results indicate a substantial improvement in inference speed while maintaining high-quality image generation. Specifically, when 25% of tokens are generated by Lumina-mGPT and the remaining 75% by MaskGIL, the generation time is reduced by 72.4%. This effectively mitigates the slow inference speed typically associated with AR models, demonstrating the efficiency of our hybrid approach.

5.2. Real-time Speech-to-Image Generation System

Any-to-English Speech Translation. Our text-driven MaskGIL model is trained on an English corpus; however, we aim to enable seamless and intuitive usage for users worldwide. To this end, we develop a speech-to-image generation system that supports over 90 languages, allowing users to generate images simply by speaking. Specifically, the core design leverages Whisper² (Radford et al., 2023), a powerful multilingual speech translation model, as an intermediary. The Whisper transcribes the user’s spoken input, translates it into English, and then directly utilizes the translated English text as

²Whisper is a general-purpose speech recognition model trained on a large-scale, diverse audio dataset. It is a multitask model capable of both multilingual speech recognition and speech translation.

a prompt for image generation, as illustrated in Figure 9.

Enhanced User Interaction. Since the speech-to-image generation system interacts directly with users, optimizing the user experience is essential. This primarily involves two key aspects: generation speed and image quality. The framework proposed in Section 5.1 is particularly well-suited for this scenario, as it enables users to balance speed and quality based on their preferences. Specifically, when prioritizing higher image quality, users can increase the contribution of the AR model, accepting potential delays in generation time. Conversely, for faster image synthesis, users can reduce the influence of the AR model, thereby accelerating the generation process.

Evaluation Data & Setup. In order to verify the effectiveness of the system, we construct a text-audio dataset, named PolyVoice³. The dataset is generated in a three-step process: (1) we employ GPT-4o to generate **English Text** \longleftrightarrow **Multilingual Text** pairs, (2) the multilingual text is synthesized into speech using Google TTS (Google, 2024), and (3) we form **English Text** \longleftrightarrow **Multilingual Audio** pairs.

The English text used for testing typically ranges from 20 to 50 words in length. Additionally, the audio data encompasses four languages: Chinese (cn), Portuguese (pt), French (fr), and Spanish (es), with each language comprising 100 audio samples. These four languages are selected for testing based on two key factors: 1) their relatively large number of speakers, and 2) their current support by Google TTS.

For evaluation, we leverage CLIPScore (Radford et al., 2021), which consists of two key metrics—Image CLIPScore and Text CLIPScore—to measure the accuracy and robustness of the system in speech-driven image generation. Image CLIPScore quantifies the similarity between images generated from audio and those generated from English text, while Text CLIPScore evaluates the semantic alignment between images generated from audio and their corresponding English text descriptions.

Evaluation Results. The evaluation results in Table 6 demonstrate that images generated from multilingual audio inputs maintain strong alignment with those generated from English text. The Image CLIPScore remains high across all languages. Similarly, the Text CLIPScore values exhibit minimal variation, indicating that the system effectively preserves semantic consistency across different languages. These results validate the system’s robustness in cross-lingual speech-to-image generation.

6. Conclusion

In this work, we explore the optimal MAR model configuration for efficient and scalable image generation. We develop a diverse set of models for class-driven image synthesis and extend our approach to support text-driven generation. Our class-driven models achieve competitive visual quality compared to widely adopted AR models while demonstrating significant efficiency gains. Simultaneously, our text-driven model preserves high visual fidelity and precise text alignment. Furthermore, we further extend our model to a broader range of applications, including: (1) accelerating AR-based generation and (2) developing a real-time speech-to-image generation system.

Table 6: Speech-to-Image Generation Performance Evaluated via CLIPScore.

Method	Image CLIP Score \uparrow	Text CLIPScore \uparrow
en text \rightarrow image	1.000	31.040
cn audio \rightarrow image	0.971	30.793
pt audio \rightarrow image	0.986	30.894
fr audio \rightarrow image	0.988	30.891
es audio \rightarrow image	0.956	30.745

³The dataset are available at <https://github.com/synbol/MaskGIL>

References

- Josh Achiam, Steven Adler, Sandhini Agarwal, Lama Ahmad, Ilge Akkaya, Florencia Leoni Aleman, Diogo Almeida, Janko Altschmidt, Sam Altman, Shyamal Anadkat, et al. Gpt-4 technical report. In *arXiv preprint arXiv:2303.08774*, 2023.
- Hangbo Bao, Li Dong, Songhao Piao, and Furu Wei. Text to image generation with bidirectional multiway transformers. *Computational Visual Media (CVM)*, 2025.
- Victor Besnier and Mickael Chen. A pytorch reproduction of masked generative image transformer. In *arXiv preprint arXiv:2310.14400*, 2023.
- Tom Brown, Benjamin Mann, Nick Ryder, Melanie Subbiah, Jared D Kaplan, Prafulla Dhariwal, Arvind Neelakantan, Pranav Shyam, Girish Sastry, Amanda Askell, et al. Language models are few-shot learners. In *Proceedings of the Advances in Neural Information Processing Systems (NeurIPS)*, 2020.
- Tom B Brown. Language models are few-shot learners. In *arXiv preprint arXiv:2005.14165*, 2020.
- Huiwen Chang, Han Zhang, Lu Jiang, Ce Liu, and William T Freeman. Maskgit: Masked generative image transformer. In *Proceedings of the IEEE Conference on Computer Vision and Pattern Recognition (CVPR)*, 2022.
- Huiwen Chang, Han Zhang, Jarred Barber, Aaron Maschinot, Jose Lezama, Lu Jiang, Ming-Hsuan Yang, Kevin Patrick Murphy, William T Freeman, Michael Rubinstein, et al. Muse: Text-to-image generation via masked generative transformers. In *Proceedings of the International Conference on Machine Learning (ICML)*, 2023.
- Junsong Chen, Jincheng Yu, Chongjian Ge, Lewei Yao, Enze Xie, Yue Wu, Zhongdao Wang, James Kwok, Ping Luo, Huchuan Lu, et al. Pixart- α : Fast training of diffusion transformer for photorealistic text-to-image synthesis. In *Proceedings of the International Conference on Learning Representations (ICLR)*, 2023.
- Mostafa Dehghani, Josip Djolonga, Basil Mustafa, Piotr Padlewski, Jonathan Heek, Justin Gilmer, Andreas Peter Steiner, Mathilde Caron, Robert Geirhos, Ibrahim Alabdulmohsin, et al. Scaling vision transformers to 22 billion parameters. In *Proceedings of the International Conference on Machine Learning (ICML)*, 2023.
- Jia Deng, Wei Dong, Richard Socher, Li-Jia Li, Kai Li, and Li Fei-Fei. Imagenet: A large-scale hierarchical image database. In *Proceedings of the IEEE Conference on Computer Vision and Pattern Recognition (CVPR)*, 2009.
- Prafulla Dhariwal and Alexander Nichol. Diffusion models beat gans on image synthesis. In *Proceedings of the Advances in Neural Information Processing Systems (NeurIPS)*, 2021.
- Ming Ding, Zhuoyi Yang, Wenyi Hong, Wendi Zheng, Chang Zhou, Da Yin, Junyang Lin, Xu Zou, Zhou Shao, Hongxia Yang, et al. Cogview: Mastering text-to-image generation via transformers. In *Proceedings of the Advances in Neural Information Processing Systems (NeurIPS)*, 2021.
- Patrick Esser, Robin Rombach, and Bjorn Ommer. Taming transformers for high-resolution image synthesis. In *Proceedings of the IEEE Conference on Computer Vision and Pattern Recognition (CVPR)*, 2021.
- Peng Gao, Le Zhuo, Ziyi Lin, Chris Liu, Junsong Chen, Ruoyi Du, Enze Xie, Xu Luo, Longtian Qiu, Yuhang Zhang, et al. Lumina-t2x: Transforming text into any modality, resolution, and duration via

- flow-based large diffusion transformers. In *Proceedings of the International Conference on Learning Representations (ICLR)*, 2025.
- Dhruba Ghosh, Hannaneh Hajishirzi, and Ludwig Schmidt. Geneval: An object-focused framework for evaluating text-to-image alignment. In *Proceedings of the Advances in Neural Information Processing Systems (NeurIPS)*, 2024.
- Google. Google text-to-speech. <https://gtts.readthedocs.io/en/latest/index.html>, 2024.
- Martin Heusel, Hubert Ramsauer, Thomas Unterthiner, Bernhard Nessler, and Sepp Hochreiter. Gans trained by a two time-scale update rule converge to a local nash equilibrium. In *Proceedings of the Advances in Neural Information Processing Systems (NeurIPS)*, 2017.
- Jonathan Ho and Tim Salimans. Classifier-free diffusion guidance. In *Proceedings of the Advances in Neural Information Processing Systems Workshops (NeurIPS Workshops)*, 2021.
- Jacob Devlin Ming-Wei Chang Kenton and Lee Kristina Toutanova. Bert: Pre-training of deep bidirectional transformers for language understanding. In *Proceedings of the Annual Conference of the North American Chapter of the Association for Computational Linguistics (NAACL)*, 2019.
- Tuomas Kynkäänniemi, Tero Karras, Samuli Laine, Jaakko Lehtinen, and Timo Aila. Improved precision and recall metric for assessing generative models. In *Proceedings of the Advances in Neural Information Processing Systems (NeurIPS)*, 2019.
- Doyup Lee, Chiheon Kim, Saehoon Kim, Minsu Cho, and Wook-Shin Han. Autoregressive image generation using residual quantization. In *Proceedings of the IEEE Conference on Computer Vision and Pattern Recognition (CVPR)*, 2022.
- José Lezama, Huiwen Chang, Lu Jiang, and Irfan Essa. Improved masked image generation with token-critic. In *Proceedings of the European Conference on Computer Vision (ECCV)*, 2022.
- Haopeng Li, Jinyue Yang, Kexin Wang, Xuerui Qiu, Yuhong Chou, Xin Li, and Guoqi Li. Scalable autoregressive image generation with mamba. In *arXiv preprint arXiv:2408.12245*, 2024a.
- Tianhong Li, Huiwen Chang, Shlok Mishra, Han Zhang, Dina Katabi, and Dilip Krishnan. Mage: Masked generative encoder to unify representation learning and image synthesis. In *Proceedings of the IEEE Conference on Computer Vision and Pattern Recognition (CVPR)*, 2023.
- Tianhong Li, Yonglong Tian, He Li, Mingyang Deng, and Kaiming He. Autoregressive image generation without vector quantization. In *Proceedings of the Advances in Neural Information Processing Systems (NeurIPS)*, 2024b.
- Bin Lin, Bin Zhu, Yang Ye, Munan Ning, Peng Jin, and Li Yuan. Video-llava: Learning united visual representation by alignment before projection. In *arXiv preprint arXiv:2311.10122*, 2023.
- Dongyang Liu, Shitian Zhao, Le Zhuo, Weifeng Lin, Yu Qiao, Hongsheng Li, and Peng Gao. Lumina-mgpt: Illuminate flexible photorealistic text-to-image generation with multimodal generative pretraining. In *arXiv preprint arXiv:2408.02657*, 2024a.
- Haotian Liu, Chunyuan Li, Qingyang Wu, and Yong Jae Lee. Visual instruction tuning. In *arXiv preprint arXiv:2304.08485*, 2023.
- Wenze Liu, Le Zhuo, Yi Xin, Sheng Xia, Peng Gao, and Xiangyu Yue. Customize your visual autoregressive recipe with set autoregressive modeling. *arXiv preprint arXiv:2410.10511*, 2024b.

- Zhuoyan Luo, Fengyuan Shi, Yixiao Ge, Yujiu Yang, Limin Wang, and Ying Shan. Open-magvit2: An open-source project toward democratizing auto-regressive visual generation. In *arXiv preprint arXiv:2409.04410*, 2024.
- AI Meta. Introducing meta llama 3: The most capable openly available llm to date. In *Meta AI*, 2024.
- OpenAI. Chatgpt: Optimizing language models for dialogue, 2022.
- OpenLM-Research. Openllama 3b. https://huggingface.co/openlm-research/open_llama_3b, 2023.
- William Peebles and Saining Xie. Scalable diffusion models with transformers. In *Proceedings of the IEEE International Conference on Computer Vision (ICCV)*, 2023.
- Shengju Qian, Huiwen Chang, Yuanzhen Li, Zizhao Zhang, Jiaya Jia, and Han Zhang. Strait: Non-autoregressive generation with stratified image transformer. In *arXiv preprint arXiv:2303.00750*, 2023.
- Qi Qin, Le Zhuo, Yi Xin, Ruoyi Du, Zhen Li, Bin Fu, Yiting Lu, Jiakang Yuan, Xinyue Li, Dongyang Liu, et al. Lumina-image 2.0: A unified and efficient image generative framework. *Proceedings of the IEEE International Conference on Computer Vision (ICCV)*, 2025.
- Alec Radford, Jong Wook Kim, Chris Hallacy, Aditya Ramesh, Gabriel Goh, Sandhini Agarwal, Girish Sastry, Amanda Askell, Pamela Mishkin, Jack Clark, et al. Learning transferable visual models from natural language supervision. In *Proceedings of the International Conference on Machine Learning (ICML)*, 2021.
- Alec Radford, Jong Wook Kim, Tao Xu, Greg Brockman, Christine McLeavey, and Ilya Sutskever. Robust speech recognition via large-scale weak supervision. In *Proceedings of the International Conference on Machine Learning (ICML)*, 2023.
- Aditya Ramesh, Mikhail Pavlov, Gabriel Goh, Scott Gray, Chelsea Voss, Alec Radford, Mark Chen, and Ilya Sutskever. Zero-shot text-to-image generation. In *Proceedings of the International Conference on Machine Learning (ICML)*, 2021a.
- Aditya Ramesh, Mikhail Pavlov, Gabriel Goh, Scott Gray, Chelsea Voss, Alec Radford, Mark Chen, and Ilya Sutskever. Zero-shot text-to-image generation. In *Proceedings of the International Conference on Machine Learning (ICML)*, 2021b.
- Ali Razavi, Aaron Van den Oord, and Oriol Vinyals. Generating diverse high-fidelity images with vq-vae-2. In *Proceedings of the Advances in Neural Information Processing Systems (NeurIPS)*, 2019.
- Robin Rombach, Andreas Blattmann, Dominik Lorenz, Patrick Esser, and Björn Ommer. High-resolution image synthesis with latent diffusion models. In *Proceedings of the IEEE Conference on Computer Vision and Pattern Recognition (CVPR)*, 2022.
- Guillaume Sanchez, Alexander Spangher, Honglu Fan, Elad Levi, and Stella Biderman. Stay on topic with classifier-free guidance. In *Proceedings of the International Conference on Machine Learning (ICML)*, 2023.
- Peize Sun, Yi Jiang, Shoufa Chen, Shilong Zhang, Bingyue Peng, Ping Luo, and Zehuan Yuan. Autoregressive model beats diffusion: Llama for scalable image generation. In *arXiv preprint arXiv:2406.06525*, 2024.

- Alpha VLLM Team. Lumina-mgpt 2.0: Stand-alone autoregressive image modeling, 2025. URL <https://github.com/Alpha-VLLM/Lumina-mGPT-2.0>.
- Chameleon Team. Chameleon: Mixed-modal early-fusion foundation models. In *arXiv preprint arXiv:2405.09818*, 2024.
- Gemini Team, Rohan Anil, Sebastian Borgeaud, Yonghui Wu, Jean-Baptiste Alayrac, Jiahui Yu, Radu Soricut, Johan Schalkwyk, Andrew M Dai, Anja Hauth, et al. Gemini: a family of highly capable multimodal models. In *arXiv preprint arXiv:2312.11805*, 2023.
- Gemma Team, Morgane Riviere, Shreya Pathak, Pier Giuseppe Sessa, Cassidy Hardin, Surya Bhatipatiraju, Léonard Hussenot, Thomas Mesnard, Bobak Shahriari, Alexandre Ramé, et al. Gemma 2: Improving open language models at a practical size. In *arXiv preprint arXiv:2408.00118*, 2024.
- Hugo Touvron, Thibaut Lavril, Gautier Izacard, Xavier Martinet, Marie-Anne Lachaux, Timothée Lacroix, Baptiste Rozière, Naman Goyal, Eric Hambro, Faisal Azhar, et al. Llama: Open and efficient foundation language models. In *arXiv preprint arXiv:2302.13971*, 2023.
- Aaron Van Den Oord, Oriol Vinyals, et al. Neural discrete representation learning. In *Proceedings of the Advances in Neural Information Processing Systems (NeurIPS)*, 2017.
- A Vaswani. Attention is all you need. In *Proceedings of the Advances in Neural Information Processing Systems (NeurIPS)*, 2017.
- Mingyang Yi, Aoxue Li, Yi Xin, and Zhenguo Li. Towards understanding the working mechanism of text-to-image diffusion model. *Proceedings of the Advances in Neural Information Processing Systems (NeurIPS)*, 2024.
- Jiahui Yu, Yuanzhong Xu, Jing Yu Koh, Thang Luong, Gunjan Baid, Zirui Wang, Vijay Vasudevan, Alexander Ku, Yinfei Yang, Burcu Karagol Ayan, et al. Scaling autoregressive models for content-rich text-to-image generation. In *Transactions on Machine Learning Research (TMLR)*, 2022.
- Lijun Yu, Jose Lezama, Nitesh Bharadwaj Gundavarapu, Luca Versari, Kihyuk Sohn, David Minnen, Yong Cheng, Agrim Gupta, Xiuye Gu, Alexander G Hauptmann, et al. Language model beats diffusion-tokenizer is key to visual generation. In *Proceedings of the International Conference on Learning Representations (ICLR)*, 2023.
- Le Zhuo, Ruoyi Du, Han Xiao, Yangguang Li, Dongyang Liu, Rongjie Huang, Wenzhe Liu, Lirui Zhao, Fu-Yun Wang, Zhanyu Ma, et al. Lumina-next: Making lumina-t2x stronger and faster with next-dit. In *Proceedings of the Advances in Neural Information Processing Systems (NeurIPS)*, 2024.
- Le Zhuo, Liangbing Zhao, Sayak Paul, Yue Liao, Renrui Zhang, Yi Xin, Peng Gao, Mohamed Elhoseiny, and Hongsheng Li. From reflection to perfection: Scaling inference-time optimization for text-to-image diffusion models via reflection tuning. *Proceedings of the IEEE International Conference on Computer Vision (ICCV)*, 2025.

Table A.1: Detailed Experimental Results of Different Image Tokenizers on the AR Paradigm. The results include FID and IS scores for various CFG settings across 50 to 200 epochs.

		50 epoch		100 epoch		200 epoch	
		FID	IS	FID	IS	FID	IS
MaskGIT-VQ (1024)	CFG = 3.0	9.8846	160.1574	9.1567	170.2633	8.7525	175.5390
	CFG = 2.5	10.2998	135.7815	9.4809	145.6140	9.1254	149.5679
	CFG = 2.0	12.6750	102.6800	11.5306	110.0108	11.2182	114.8622
Chameleon-VQ (8192)	CFG = 3.0	8.5799	180.8341	8.1700	193.9580	7.5208	200.0188
	CFG = 2.5	8.9955	153.5894	8.2882	165.1865	7.7708	175.9126
	CFG = 2.0	11.6736	115.8210	10.5847	125.7858	9.6992	133.8924
LlamaGen-VQ (16384)	CFG = 3.0	9.2867	199.3415	8.8726	215.3014	8.0206	221.3254
	CFG = 2.5	8.2499	171.4478	7.7843	185.0560	6.8314	191.7435
	CFG = 2.0	8.7104	133.0047	7.8188	144.1255	7.0980	149.0620
Open-MAGVIT2-VQ (262144)	CFG = 3.0	10.9688	129.7520	10.8770	131.0903	9.5125	146.1105
	CFG = 2.5	15.5837	96.4929	14.8460	100.0897	14.8755	100.2676
	CFG = 2.0	25.2163	63.6719	24.1729	66.1162	22.7751	71.5757

A. Detailed Evaluation Results of Discrete-Value Image Tokenizer

Table A.2: Detailed Experimental Results of Different Image Tokenizers on the MAR Paradigm. The results include FID and IS scores for various CFG settings across 50 to 200 epochs.

			MaskGIT-VQ (1024)			Chameleon-VQ (8192)			LlamaGen-VQ (16384)			Open-MAGVIT2-VQ (262144)		
			CFG = 3.0	CFG = 2.5	CFG = 2.0	CFG = 3.0	CFG = 2.5	CFG = 2.0	CFG = 3.0	CFG = 2.5	CFG = 2.0	CFG = 3.0	CFG = 2.5	CFG = 2.0
Bidirectional Transformer	50 epoch	FID	16.6349	17.9747	20.2007	16.9894	19.3724	22.9273	15.4235	16.9273	19.2510	90.4830	94.1686	98.6222
		IS	98.2236	89.0695	76.8371	106.1228	92.8579	78.0924	114.4028	100.5291	86.2001	15.1394	14.1799	13.0694
	100 epoch	FID	12.4982	13.6014	15.5298	11.4843	12.7807	15.2883	10.7954	10.8447	11.6757	57.7810	64.0669	71.2787
		IS	128.8805	114.9444	99.3552	148.9279	133.6862	112.5623	173.5138	156.9519	136.1681	31.4727	26.7601	22.9549
	200 epoch	FID	9.9150	10.8601	12.6045	8.5408	9.3071	11.2243	8.9188	8.4767	8.5895	32.8960	43.2282	51.0961
		IS	154.5364	136.8136	115.7622	189.5333	169.3695	145.7171	213.7065	193.9830	169.5869	64.8568	45.3654	36.6035
	50 epoch	FID	12.5828	13.3734	14.7296	10.6284	11.3143	12.9145	9.8001	9.7923	10.1693	12.5832	14.9028	18.8675
		IS	121.7072	109.3891	96.8131	144.3818	130.8738	114.3169	169.3604	152.9462	136.0035	121.8998	104.8236	86.8462
Bidirectional LLaMA	100 epoch	FID	9.4469	9.9894	10.9635	8.3184	8.4573	9.4030	8.1221	7.8057	7.7422	9.1883	11.2308	14.6781
		IS	160.4776	143.2989	126.3950	188.8565	172.2684	152.5737	213.7423	194.7384	174.4664	153.0440	131.4824	108.0728
	200 epoch	FID	7.9954	8.3240	8.8536	6.7024	6.6765	7.2351	6.9971	6.4922	6.1397	7.1548	8.4162	9.3161
		IS	191.4879	173.8534	154.6600	226.5536	206.9128	185.9040	244.6256	222.4675	201.6035	214.9400	172.6521	155.9095

A.1. Results on Autoregressive Generation

We present detailed experimental results for various image tokenizers applied to the autoregressive (AR) paradigm in Table A.1. These experiments are conducted using the Casual LLaMA architecture and evaluated on the class-conditional ImageNet-1k benchmark. The results include FID and IS scores measured at 50, 100, and 200 epochs under CFG settings of 3.0, 2.5, and 2.0. Among these tokenizers, LlamaGen-VQ with a codebook size of 16,384 outperforms the others. For a comprehensive analysis, please refer to Section 3.1 in the main paper.

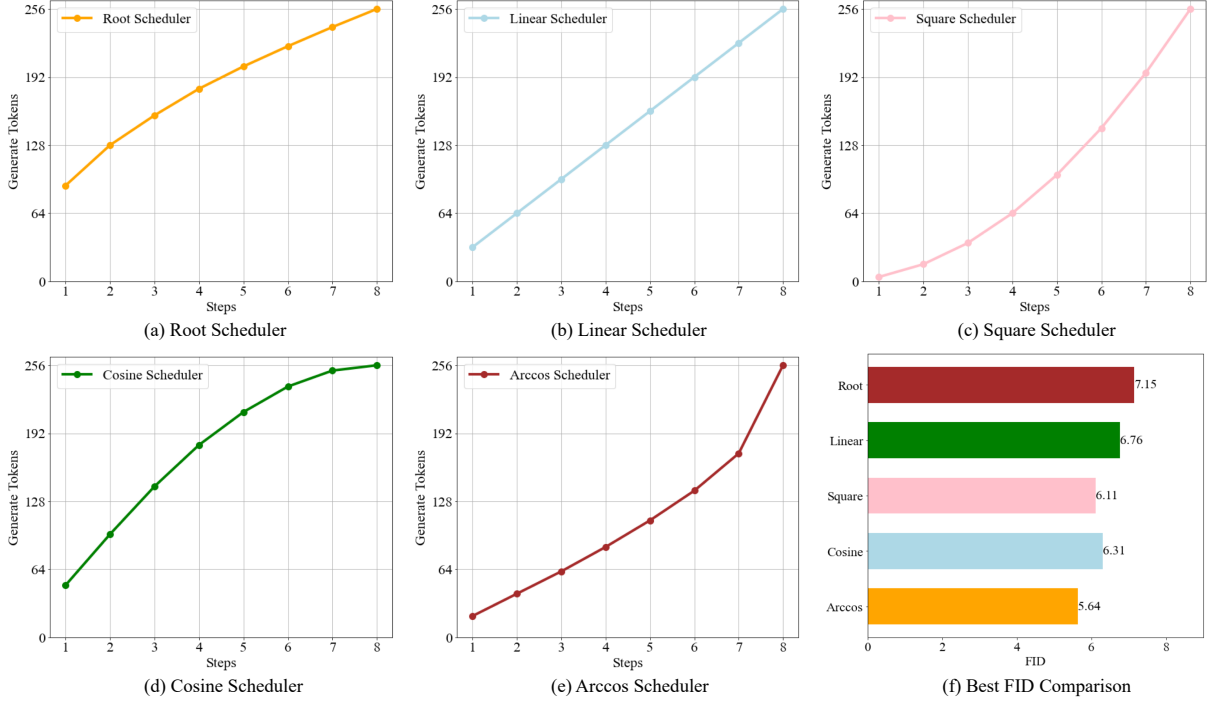


Figure A.1: Scheduler Configurations and Metrics on Imagenet 256×256 Benchmark.

A.2. Results on Mask Autoregressive Generation

We present detailed experimental results for various image tokenizers applied to the masked autoregressive (MAR) paradigm in Table A.2. These experiments utilize the Bidirectional LLaMA and Bidirectional Transformer models, evaluated on the class-conditional ImageNet-1k benchmark. The results report FID and IS scores across 50, 100, and 200 epochs under CFG settings of 3.0, 2.5, and 2.0. Among these tokenizers, LlamaGen-VQ demonstrates the best performance for the MAR paradigm. From a model architecture perspective, the Bidirectional LLaMA achieves superior results. For a more detailed analysis, refer to Section 3.1 in the main paper.

Table A.3: Detailed Experimental Results of Scaling MaskGIL. The results include FID and IS scores for various CFG settings across 50 to 400 epochs.

		MaskGIL-B (111M)				MaskGIL-L (343M)				MaskGIL-XL (775M)				MaskGIL-XXL (1.4B)		
		CFG = 3.0	CFG = 2.5	CFG = 2.0	CFG = 1.5	CFG=3.0	CFG=2.5	CFG=2.0	CFG=1.5	CFG=3.0	CFG=2.5	CFG=2.0	CFG=1.5	CFG=3.0	CFG=2.5	CFG=2.0
50 epoch	FID	9.8001	9.7923	10.1693	11.4326	8.1032	7.3123	6.7532	6.9289	5.9404	5.4523	5.4149	6.4069	4.9994	4.6997	5.0216
	IS	169.3604	152.9462	136.0035	115.6833	248.7714	229.2365	204.0812	172.9692	259.9695	235.1068	204.2972	172.1452	277.6597	251.9433	218.3809
100 epoch	FID	8.1221	7.8057	7.7422	8.2393	6.8974	5.8711	5.3028	5.2657	4.7785	4.2401	4.2148	5.2318	3.8788	4.0727	4.8170
	IS	213.7423	194.7384	174.4664	150.8941	287.1859	265.8999	235.5590	203.3373	299.0290	271.2699	237.7044	198.0010	285.9541	255.0303	220.0994
200 epoch	FID	7.4975	6.4922	6.1397	6.8546	6.2931	5.7252	4.8876	4.5048	4.2346	3.9977	4.1228	5.5923	3.9649	3.8788	4.4784
	IS	244.6256	222.4675	201.6035	169.0343	327.0787	303.9240	275.0859	235.0050	314.0859	281.0844	262.0203	205.5776	305.9541	274.0724	240.9620
300 epoch	FID	6.9971	6.3837	5.6994	5.6713	6.1342	5.1874	4.5432	4.3718	4.1886	3.9442	4.0512	4.9251	3.8365	3.7199	4.2015
	IS	271.4360	250.5148	226.8228	194.3450	331.4310	306.8823	272.2563	236.6083	321.1712	291.0879	259.2443	220.4716	306.6679	282.4760	253.4782
400 epoch	FID	7.0901	6.2576	5.6450	5.6713	5.4711	4.6372	4.0185	4.0854	4.0931	3.9031	4.0522	4.7214	/	/	/
	IS	274.9196	255.3847	229.9646	199.2374	336.8414	312.2809	281.1118	239.8479	326.2475	296.2475	269.8136	237.9921	/	/	/

Table A.4: Detailed Experimental Results Under Different Decoding Steps and Different Schedulers. This experiment shows the checkpoint results of MaskGIL-B at 400 epochs, with CFG= 2.0.

	4 Steps		8 Steps		16 Steps		32 Steps		64 Steps	
Scheduler	FID	IS	FID	IS	FID	IS	FID	IS	FID	IS
Root	9.4683	177.5355	7.1539	250.1702	9.1172	240.3087	10.3262	225.1267	10.8516	207.2014
Linear	10.9076	162.2468	6.7640	239.9988	8.6355	233.0458	9.8178	216.4662	10.5585	204.8842
Square	13.4522	141.6912	6.1144	227.3088	7.9051	226.6961	9.2745	213.4663	10.0068	201.7469
Cosine	12.8029	145.7202	6.3108	230.7038	8.2024	228.5306	9.5711	214.4882	10.1930	201.3121
Arccos	13.2392	143.9644	5.9056	220.2331	7.3303	217.5756	8.3202	205.5842	9.5981	195.7871

B. Details of Mask Schedulers

We evaluate five mask schedulers, including root, linear, square, cosine, and arccos. To provide an intuitive understanding of the differences between these schedulers, we plot the number of generated tokens at each generation step, as illustrated in Figure A.1.

C. Detailed Evaluation Results of Different Decoding Steps

To explore how the number of decoding steps impacts generation quality, we perform an ablation study on the class-conditional ImageNet benchmark, with findings summarized in Table A.4. From the results, all mask schedulers present the same conclusion, that is, increasing the number of decoding steps does not consistently enhance generation quality. Notably, 8-step decoding achieves the best results across all mask schedulers.

D. Detailed Evaluation Results of Scaling MaskGIL

In this work, we scale the model parameters of MaskGIL from 111M to 1.4B. Table A.3 details the FID and IS scores for each model size at various training epochs and CFG settings. Notably, the results for our MaskGIL-XXL currently cover only up to 300 epochs. Notable improvements in FID are observed when scaling the model from MaskGIL-B to MaskGIL-XXL. For a detailed analysis, please refer to Section 4.